Supporting information for

High-Efficiency Peroxidase Mimics for Fluorescence Detection of H_2O_2 and L-cysteine

Xiaodan Qu,[1,2,3] Jinhui Zou,[3] Yujie Shen,[3] Bolin Zhao,[3,4] Jiahui Liang,[3] Zhenxin Wang,[1,2] Yuwei Zhang,*[3] and Li Niu*[3,4]

[1] *State Key Laboratory of Electroanalytical Chemistry, Changchun Institute of Applied Chemistry, Chinese academy of science, Changchun, Jilin, 130022, P.R. China*

[2] *University of Science and Technology of China, Hefei, Anhui, 230026, P.R. China*

[3] *Center for Advanced Analytical Science, c/o School of Chemistry and Chemical Engineering, Guangzhou Key Laboratory of Sensing Materials & Devices, Guangzhou University, Guangzhou, Guangdong, 510006, P. R. China*

[4] *School of Civil Engineering, Guangzhou University, Guangzhou, Guangdong, 510006, P. R. China*

Experimental Section

Chemicals and Materials. Chloroauric acid tetrahydrate ($HAuCl_4 \cdot 4H_2O$) was from Sinopharm Group Chemical Reagent Co.,Ltd. (Shanghai, China). Silver nitrate ($AgNO_3$) was from Shanghai Chemical Reagent Co. Ltd. (Shanghai, China). Potassium dihydrogen phosphate (KH_2PO_4), dibasic sodium phosphate (Na_2HPO_4), sodium citrate dihydrate ($C_6H_5Na_3O_7 \cdot 2H_2O$), hydrogen peroxide solution (H_2O_2) and isopropyl alcohol (C_3H_8O) were perchased from Guangzhou Chemical Reagent Factory (Guangzhou, China). Amplex Red (AR), cysteine (cys), histidine, threonine, tyrosine, glycine, phenylanine, lyscine, glutamic acid, glucose and proline were all obtained from Aladdin Chemistry Co. Ltd. (Shanghai, China). All chemicals were obtained from commercial sources and used without any further purification. Double distilled water was used for the preparation of all the solutions.

Instruments. The pH measurements were performed with a pH-meter FE-28 (METTLER TOLEDO). X-ray photoelectron spectroscopy (XPS) was conducted on a ESCALABMKII X-ray photoelectron spectrometer with a monochromatic Al Ka X-ray source. UV-vis spectra were recorded using an Agilent Cary 60 UV-vis spectrophotometer. Fluorescence measurements were investigated via F-4600 Hitachi spectrometer. High-resolution transmission electron microscopy (HRTEM) image and TEM image were obtained by JOEL JEM-2100F TEM/STEM operating at 200 kV. The powder X-ray diffraction (XRD) patterns were recorded on a PANalytical PW3040/60 diffractometer equipped with a Cu Ka radiation source. A Bruker EMXnano ESR spectrometer was used for Electron spin resonance (ESR) measurement, and DMPO was choosed to trap radicals.

Synthesis of Au@AuAg NPs. Au@AuAg NPs with different shell thickness were synthesized according to a modified seeded growth approach.[1, 2] Briefly, an aqueous solution of 0.01% $HAuCl_4$ (200 mL) was heated to boiling point with vigorous stirring, and then 1% trisodium citrate solution (2.0 mL) was quickly injected to the solution. The color of the mixed solution turned from yellow to black and finally wine-red which means the formation of Au seeds. After keeping boiling for another 10 min, stirring was continued and the reaction mixture was cooled to room temperature.

The solution of $AgNO_3$ (5 mg/mL, 400 μL) was added while the as-synthesized citrate-capped Au seeds solution (20 mL) was refluxed at 135 ℃. Subsequently, 1% trisodium citrate was added dropwise and keep the solution refluxed for 30 min. The solution was cooled down and the final volume was made up to 20 mL. The concentration of $AgNO_3$ solution (5, 7, 9, 11 mg/mL) added into the reaction mixture was varied to finely control the Ag shell thichness of resulting NPs. The concentrations of Au@AuAg NPs were calculated to be about 5.2×10^{-10} M.[3]

Evaluation of peroxidase-like activity. The enzyme-like activities of Au@AuAg NPs were evaluated by the steady-state kinetic assays. All the assays were conducted in 0.01 M phosphate buffers solution (PBS), pH 7.4. In a typical assay, 5.2×10^{-11} M Au@AuAg NPs were mixed with 1 mM H_2O_2 and different concentrations of AR in PBS and the fluorescence emission intensity at 585 nm of the obtained solutions were then collected by setting the excitation wavelength at 540 nm. Then the fluorescence intensity versus time curve was obtained. The standard equation for resorufin concentration and fluorescence intensity was $Y = 430.74X + 47.47$ and the reaction velocity (v) can be derived through the equation: $v = \text{Slope}/430.74$ a.u. μM^{-1}. Then the plot of reaction velocity against AR concentration (Fig. 2b) can be obtained and fitted by the Michaelis-Menten equation $v = V_{max} x[S]/(K_m + [S])$, where V_{max} is the maximal reaction velocity, [S] is the concentration of AR and K_m is the Michaelis constant. The catalytic efficiency (K_{cat}) can be obtained from the equation: $K_{cat} = V_{max}/[E]$, where [E] is the particle concentration of catalysts. The area-specfic catalytic efficiency ($K_{cat\text{-}specific}$ can be derived by the equation: $K_{cat\text{-}specific} = K_{cat}/S$, where S is the surface area of an individual NP.

Fluorescence detection of H_2O_2 and Cys. The typical assays of H_2O_2 were performed as follow: 1.5 mL of PBS buffer (pH 7.4) containing 0.13 mM AR, 3.46×10^{-11} M $Au@AuAg_9$ NPs, different concentration of H_2O_2 was incubated for 30 min under argon. The fluorescence spectrum of resulting solution was monitored at 585 nm. Moreover, a fluorescence detection for Cys can be developed. Varied concentration of Cys was injected into the PBS solution containing fixed concentrations of H_2O_2 (1.6 mM) and AR (0.19 mM). After reaction for 10 min at the room temperature, the fluorescence intensity at 585 nm was monitored. Common potentially interfering amino acids (including histidine, threonine, tyrosine, glycine, phenylanine, lyscine, glutamic acid and proline) and glucose whose concentrations were fixed at 2 μM were used to replace Cys to investigate the selectivity of this fluorescence detection method.

Trapping experiment. To investigate the catalytic mechanism of Au@AuAg NPs, trapping experiments were performed using isopropanol (13 mM) as ·OH scavenger. The fluorescence intensity of solutions containing AR, H_2O_2, Au@AuAg and isopropanol was compared with that of reaction solutions without isopropanol.

DFT calculation. The charge density difference images were obtained by VESTA visualization software and calculated as $\Delta\rho(r) = \rho_{total(r)} - \rho_{support} - \rho_{molecule(r)}$, where the $\rho_{total(r)}$ is the electron density of the AR or H_2O_2 molecule adsorbed on the support, the $\rho_{support}$ is the electron density of the support, and the $\rho_{molecule(r)}$ is the electron density of the adsorbed molecule. The calculated structure models of support adopted the (111) surface with the atom ratio of 5 Ag : 1 Au according to the XPS analysis.

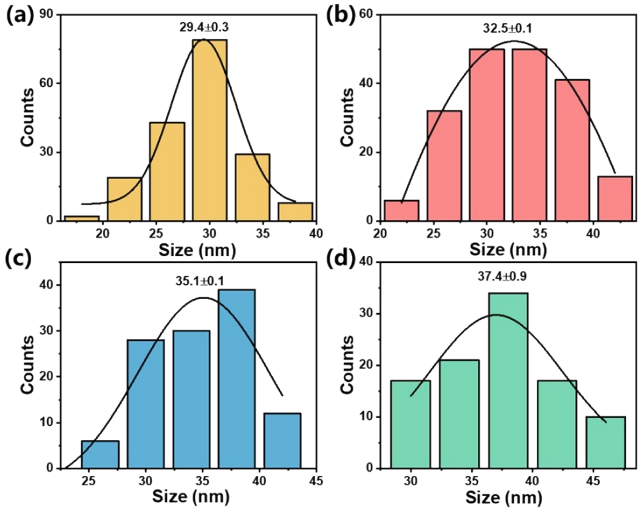

Figure S1. The histograms of size distribution of Au@AuAg NPs: (a) Au@AuAg-5; (b) Au@AuAg-7; (c) Au@AuAg-9; (d) Au@AuAg-11.

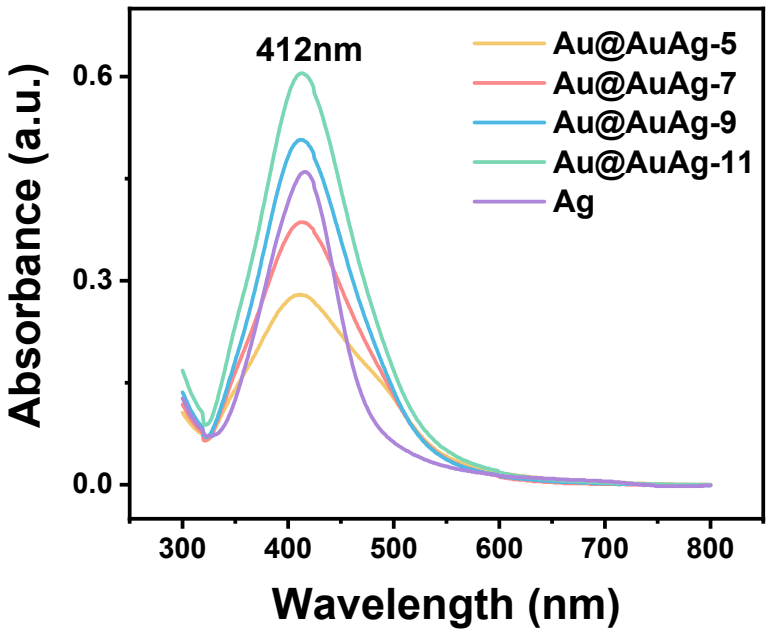

Figure S2. UV-vis absorotion spectra of Au@AuAg NPs and Ag NPs.

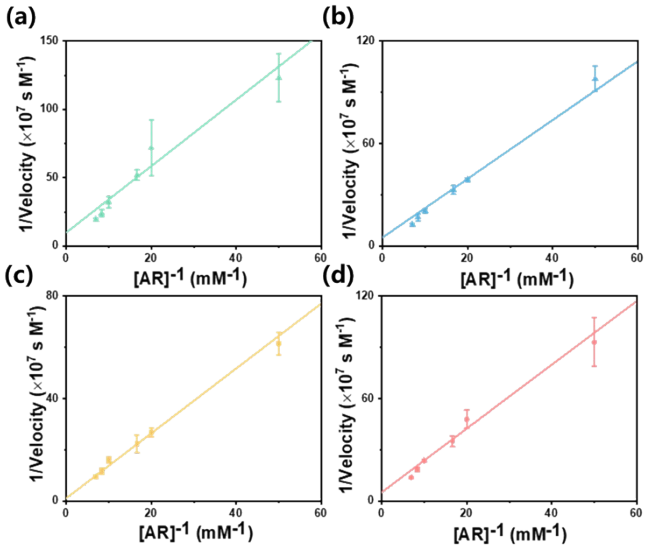

Figure S3. Double-reciprocal plots for: (a) Au@AuAg-5; (b) Au@Au Ag-7; (c) Au@Au Ag-9; (d) Au@Au Ag-11 that were generated from Fig. 2b. Error bars are the standard deviations of three independent experiments.

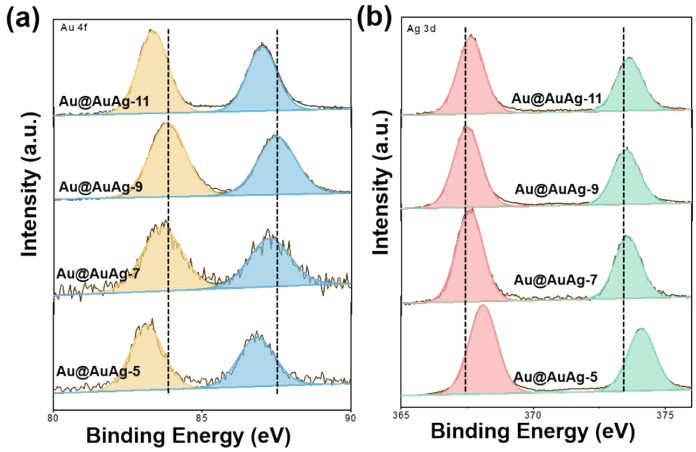

Figure S4. High-resolution XPS spectra of (a) Au 4f, and (b) Ag 3d for AuAg@Au-x (x=5, 7, 9, 11).

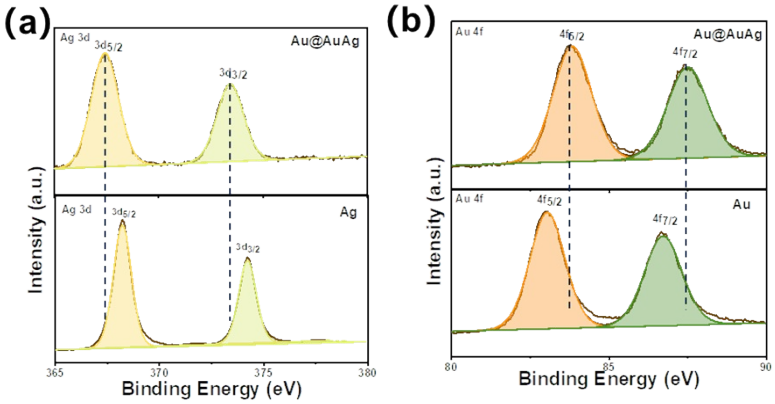

Figure S5. (a) Ag 3d XPS spectra of Ag NPs and Au@Ag NPs. (b) Au 4f XPS spectra of Au NPs and Au@Ag NPs.

Both H_2O_2 and AR prefer adsorbing on the Ag sites of Au@AuAg NPs surface instead of the Au sites. According to the previous studies, in the single-molecule experiment, the average product formation rate $\langle\tau_{off}\rangle^{-1}$ (Figure S6a) first increases with the increase of [AR], and subsequently decreases above a certain concentration (6 nM), suggesting a competitive adsorption mechanism on Au@AuAg NPs surface (Figure S6b).[4] This means that the active sites could active both AR and H_2O_2 molecules. To further clarify the active sites, the density functional theory (DFT) calculation was carried out to discuss the adsorption energy of AR and H_2O_2 on Au and Ag sites in the catalytic process. According to the DFT calculation results in Table S3 (Part of the data comes from the previous studies[4]), H_2O_2 cannot be chemically adsorbed on the Au sites. This means that Au sites have no ability to activate H_2O_2. It can be reasonably inferred that Au sites on Au@AuAg NPs surface are not active sites. In addition, AR on Ag sites has greater adsorption energy than that on Au sites. This also indicates that AR is prefer to be adsorbed and activated on Ag sites. In summary, both H_2O_2 and AR prefer adsorbing on the Ag sites of Au@AuAg NPs surface which work as active sites.

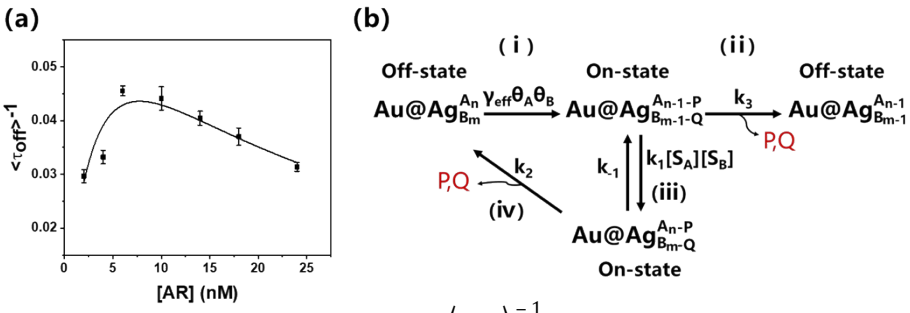

Figure S6. (a) AR concentration dependence of product formation rates ($\langle\tau_{off}\rangle^{-1}$) on Au@AuAg NPs. Solid lines are fitted with Equation 1, 2, 3, and 4, respectively. Every data is the average of the turnover trajectories of more than 70 NPs. Error bar = S.E.M. (f) Diagram of the kinetic mechanism of a catalytic turnover on Au@AuAg NPs. A, B, P, and Q denote AR, H_2O_2, resorufin, and H_2O molecules, respectively; n and m represent the number of AR molecules and H_2O_2 molecules adsorbed on the NP surface in the equilibrium state, respectively.

Table S1. The surface atomic composition (%) measured by XPS.

Materials	**Au**	**Ag**
Au@AuAg-5	14.78	85.22
Au@AuAg-7	18.71	81.29
Au@AuAg-9	23.23	76.77
Au@AuAg-11	21.63	78.37

Table S2. Comparison of the kinetic parameters of different catalysts toward the oxidation of AR by H_2O_2. K_m is the Michaelis constant, V_{max} is the maximal reaction velocitiy, K_{cat} is the catalytic constant, S is the surface area of an individual NP, and $K_{cat\text{-}specific}$ is the specific-area catalytic efficiency.

Materials	V_{max} **(x 10^{-8} M s^{-1})**	K_m **(x 10^{-4} M)**	K_{cat} **(x 10^{2} s^{-1})**	***S*** **(x 10^{4} nm^2)**	$K_{cat\text{-}specific}$ **(x 10^{-2} s^{-1} nm^{-2})**
Au@AuAg-5	1.02	2.48	1.96	1.09	1.81
Au@AuAg-7	2.00	3.44	3.84	1.33	2.89
Au@AuAg-9	9.20	11.66	17.68	1.55	11.42
Au@AuAg-11	1.95	3.65	3.76	1.76	2.14

Table S3. Adsorption energy calculated by DFT.

Catalyst sites	E_{abs} **(H_2O_2) [eV]**	E_{abs} **(AR) [eV]**
Au sites	[a]None	-1.56
Ag sites	[b]-0.28	[c]-2.26

Notes: a represents that the calculation result could not be obtained as H_2O_2 molecules could not be adsorbed on Au sites. b and c represent the corresponding data that comes from our previous studies[4].

Table S4. Comparison of different materials peroxidase mimics-based sensing platforms for H_2O_2 detection.

Materials	***Linear range*** **(μM)**	***Detection limit*** **(μM)**	***Refs***
N/S CDs	10-100	1.75	[5]
VS_4	50-300	5	[6]
PDI/CeO_2 NR	10-500	2.23	[7]
PEI-AgNC	0.1-20	0.035	[8]
PtS_2	1-100	0.33	[9]
RFP/Ag NPRs	1-120	0.28	[10]
Au@AuAg	1-400	0.864	This work

Table S5. Comparison of different materials peroxidase mimics-based sensing platforms for Cys detection.

Materials	***Linear range*** **(μM)**	***Detection limit*** **(μM)**	***Refs***
MoS_2-Au@Pt	0.8-400	0.5	[11]
$NiMo_6$@Co_3O_4	1-20	0.018	[12]
GSH-Au/Pt NCs	0.5-30	0.154	[13]
VS_4	5-100	2.5	[6]
CeO_2/CoO NCs	5-10	3.71	[14]
FeOCl NSs	3-33	2.76	[15]
Au@AuAg	0.075-2	0.035	This work

Table S6. Determination of Cys in real sample.

Sample	*Found without spiking* (μM)	*Spiked Cys* (μM)	Obtained (μM)	*Recovery* (%)	*RSD* (%)
Honey	0.50	0.10	0.61	100.95	0.70
	0.50	0.50	0.99	99.34	2.32
	0.50	0.90	1.35	96.92	7.87
Tap water	0.00	0.15	0.17	110.29	1.41
	0.00	0.40	0.39	98.79	0.31
	0.00	0.60	0.61	101.71	0.55

References

1 M.-S. Wu, L.-J. He, J.-J. Xu and H.-Y. Chen, *Anal. Chem.*, 2014, **86**, 4559-4565.
2 W.-S. Zhang, J.-T. Cao, Y.-X. Dong, H. Wang, S.-H. Ma and Y.-M. Liu, *J. Lumin.*, 2018, **201**, 163-169.
3 W. T. Haiss, N. T. K. Aveyard and J. Fernig D. G., *Anal. Chem.*, 2007, **79**, 4215-4221.
4 X. Qu, B. Zhao, W. Zhang, J. Zou, Z. Wang, Y. Zhang and L. Niu, *J. Phys. Chem. Lett.*, 2022, https://doi.org/10.1021/acs.jpclett.1c03854.
5 M. Tang, B. Zhu, Y. Wang, H. Wu, F. Chai, F. Qu and Z. Su, *Mikrochim. Acta*, 2019, **186**, 604.
6 C. Chen, Y. Wang and D. Zhang, *Mikrochim. Acta*, 2019, **186**.
7 H. Liu, Y. He, N. Li, Z. Liu, X. Zhang, X. Zhang and Q. Liu, *ACS Appl. Bio. Mater.*, 2020, **3**, 2499-2506.
8 T. Zhou, Z. Su, X. Y. Wang, M. C. Luo, Y. F. Tu and J. L. Yan, *Spectroc. Acta Pt. A*, 2021, **244**, 6.
9 W. Zhang, X. Li, T. Cui, S. Li, Y. Qian, Y. Yue, W. Zhong, B. Xu and W. Yue, *Mikrochim. Acta*, 2021, **188**, 174.
10 H. Lu, C. Yu, Y. Zhang and S. Xu, *Anal. Chim. Acta*, 2019, **1048**, 178-185.
11 L. Wan, L. Wu, S. Su, D. Zhu, J. Chao and L. Wang, *Chem. Commun.*, 2020, **56**, 12351-12354.
12 M. Xu, X. Li, J. Q. Sha, Z. Tong, Q. Li and C. Liu, *Chemistry*, 2021, **27**, 9141-9151.
13 J. J. Li, D. Qiao, S. Z. Yang, G. J. Weng, J. Zhu and J. W. Zhao, *Spectroc. Acta Pt. A*, 2021, **248**, 119257.
14 J. Lian, P. Liu, C. Jin, Q.-Y. Liu, X. Zhang and X. Zhang, *ACS Sustain. Chem. Eng.*, 2020, **8**, 17540-17550.
15 Z. Mohammadpour, F. Malekian Jebeli and S. Ghasemzadeh, *Mikrochim. Acta*, 2021, **188**, 239.